JCTC Journal of Chemical Theory and Computation

Quantum Chemical Benchmark Studies of the Electronic Properties of the Green Fluorescent Protein Chromophore. 1. Electronically Excited and Ionized States of the Anionic Chromophore in the Gas Phase

Evgeny Epifanovsky,*,† Igor Polyakov,‡ Bella Grigorenko,‡ Alexander Nemukhin,‡,§ and Anna I. Krylov*,†

Department of Chemistry, University of Southern California, Los Angeles, California 90089, Department of Chemistry, M.V. Lomonosov Moscow State University, Moscow 119991, Russia, and Institute of Biochemical Physics, Russian Academy of Sciences, Moscow 119334, Russia

Received March 25, 2009

Abstract: We present the results of quantum chemical calculations of the electronic properties of the anionic form of the green fluorescent protein chromophore in the gas phase. The vertical detachment energy of the chromophore is found to be 2.4−2.5 eV, which is below the strongly absorbing $\pi\pi^*$ state at 2.6 eV. The vertical excitation of the lowest triplet state is around 1.9 eV, which is below the photodetachment continuum. Thus, the lowest bright singlet state is a resonance state embedded in the photodetachment continuum, whereas the lowest triplet state is a regular bound state. Based on our estimation of the vertical detachment energy, we attribute a minor feature in the action spectrum as due to the photodetachment transition. The benchmark results for the bright $\pi\pi^*$ state demonstrated that the scaled opposite-spin method yields vertical excitation within 0.1 eV (20 nm) from the experimental maximum at 2.59 eV (479 nm). We also report estimations of the vertical excitation energy obtained with the equation-of-motion coupled cluster with the singles and doubles method, a multireference perturbation theory corrected approach MRMP2 as well as the time-dependent density functional theory with range-separated functionals. Expanding the basis set with diffuse functions lowers the $\pi\pi^*$ vertical excitation energy by 0.1 eV at the same time revealing a continuum of "ionized" states, which embeds the bright $\pi\pi^*$ transition.

1. Introduction

Unique electronic properties of the green fluorescent protein (GFP) whose natural function is to convert blue light to green light have motivated a number of experimental and theoretical studies and have been exploited in numerous practical applications.[1−3] Due to their fundamental and practical importance, studies of the structure and properties of photoreceptor proteins and their denatured chromophores constitute an important field of modern research. Moreover, GFP can be considered as a model for other fluorogenic unsymmetric methine dyes[4−9] and is of interest to organic photovoltaic materials. For example, the fluorescent protein motif has already inspired the creation of new organic phototovoltaic sensitizers[10] and other optoelectronic materials.[11]

From the theoretical perspective, characterization of the electronic structure of isolated chromophores is the first step toward understanding their photochemical and photobiological properties in realistic environments. Modeling isolated species involves calculating the molecular parameters of the chromophores in the gas phase and in solution using quantum

* Corresponding authors. E-mail: epifanov@usc.edu (E.E.) and krylov@usc.edu (A.I.K.).
† University of Southern California.
‡ M.V. Lomonosov Moscow State University.
§ Russian Academy of Sciences.

10.1021/ct900143j CCC: $40.75
Published on Web 06/25/2009

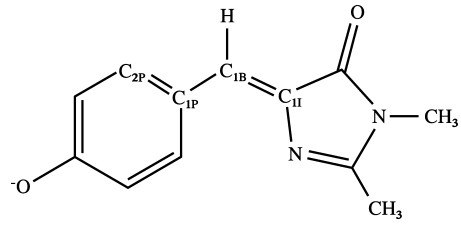

Figure 1. Chemical structure and atomic labels of the anionic form of the model GFP chromophore HBDI in the *cis*-conformation.

chemistry methods. This series of two papers focuses on accurate calculations of the properties of biological chromophores with ab initio methods using the model GFP chromophore, 4′-hydroxybenzylidene-2,3-dimethylimidazolinone (HBDI) anion, as a benchmark system (Figure 1). In this paper, we present the vertical excitation and electron detachment energies and discuss the electronic properties of the excited and detached states. In a subsequent paper,[12] we discuss the *cis*−*trans* isomerization of the HBDI anion in the ground electronic state.

Earlier experimental studies have characterized the absorption of HBDI in the native protein environment.[13] The spectrum of the wild-type GFP has two broad absorption bands at 396 nm (3.13 eV) and 476 nm (2.60 eV) assigned to the neutral and anionic forms of the chromophore, respectively. The spectra in aqueous solution[14,15] reveal strong pH sensitivity: the absorption maximum at neutral pH is at 370 nm (3.35 eV), whereas at pH = 13 and pH = 1, it is shifted to 426 nm (2.91 eV) and 396 nm (3.13 eV), respectively. The absorption of denatured wild-type proteins exhibits a similar pH-dependence.[16] The shifts were attributed to different protonation and deprotonation forms, as well as a strong interaction with water. The latter is consistent with a large change (about 7 D) of the dipole moment upon excitation determined in the Stark effect measurements taken in a buffered (pH = 6.5) glycerol solution at 77 K.[17] Therefore, the protonation and deprotonation of HBDI and the solvent effects, which strongly affect its electronic properties, needed to be accounted for in theoretical models. However, it is important to characterize the chromophore in the gas phase first in order to quantify the solvent effect separately.

Recently, a gas-phase action spectrum of anionic HBDI (as well as other protonated forms), using photodestruction spectroscopy of mass-selected ions injected into an electrostatic ion storage ring, was reported providing an important reference for theory.[14,15] The spectrum shows an absorption band centered at 2.59 eV (479 nm), which extends from 2.4−2.8 eV (440−520 nm) as well as a minor peak around 2.3 eV (540 nm). The authors emphasized a striking similarity between the absorption bands in the gas phase and the protein and suggested that the protein environment shields the chromophore from water and that the absorption in the protein is an intrinsic property of HBDI. While the role of the protein still needs to be investigated, this measurement facilitates more direct comparison between the gas-phase calculations of vertical excitation energies and the experimental absorption for benchmarking theoretical methods.

The large absorption band in the gas-phase spectrum of the HBDI anion has been assigned as the $\pi\pi^*$ transition, however, the nature of the minor feature at 2.3 eV has not been discussed.

A variety of electronic structure techniques ranging from simple semiempirical approximations to high-level ab initio methods have been applied to simulate the properties of the *cis*-anionic form of HBDI.[18−24] Selected representative results are summarized in Table 1.

These studies have identified the absorbing state of the HBDI anion as the S_1 state derived from a HOMO−LUMO excitation of the $\pi\pi^*$ character. LUMO, however, is a valence π^*-like orbital only in relatively small basis sets; including diffuse functions increases the number of molecular orbitals between the HOMO and the lowest π^*-like orbital. Although the bright state retains its $\pi\pi^*$ character, it is not, strictly speaking, a HOMO−LUMO transition in a realistic basis set.

The first theoretical studies on the chromophore, dating back to the late 1990s,[18,19] employed semiempirical methods based on the neglect-of-differential overlap approximation. They placed the $\pi\pi^*$ state at 2.77 eV or 0.18 eV above the experimental absorption maximum. Ab initio calculations using configuration interaction with single excitations (CIS) in a small basis set[20] grossly overestimated the excitation energy. These and other results from Table 1 reveal that accurate calculations of the vertical excitation energy for the bright $\pi\pi^*$ transition are challenging for quantum chemistry.

Time-dependent density functional theory (TD-DFT), which can be applied to very large systems, gave rise to high expectations in the field of photochemistry. However, the notorious self-interaction error[25−27] results in an unphysical description of charge-transfer (CT) states,[28] which are common in large molecules. In addition to artificially low excitation energies of real CT states, spurious CT states appear, spoiling the description of other states. The number of these false states increases steeply with the system size.[29] In the case of fluorescent protein chromophores, TD-DFT has been reported to perform quite modestly, as discussed in ref 23. In that study, which examined various functionals, the best agreement with the experiment was obtained for the BP86 functional.[30,31] This value, 2.94 eV (421 nm), which is listed in Table 1, is still 0.35 eV (60 nm) away from the experiment. Overall, TD-DFT excitation energies range from 2.94 to 3.23 eV,[23] the popular B3LYP functional[32,33] yields 3.05 eV.

CASPT2, the complete active space self-consistent field (CASSCF) method with second-order perturbation theory (PT2) correction,[34] has been applied to model photochemical properties of organic chromophores in various media.[22,35−44] The CASPT2/6-31G(d) result[22] from Table 1 agrees fairly well with the experimental value; however, the CAS distribution of 12 electrons over 11 orbitals is a truncation of the entire π-orbital active space, which requires the CASSCF(16/14) wave function for the GFP chromophore. Bravaya et al.[24] performed calculations of the vertical $\pi\pi^*$ transition energies for various forms of HBDI using a very expensive and highly correlated approach, i.e., state-averaged CASSCF(16/14) wave functions constructed in the full π-orbital active space augmented by perturbative corrections:

Table 1. Selected Theoretical Estimates of the S_0-S_1 Vertical Excitation Energy (ΔE) and the Corresponding Wavelengths for the Gas-Phase GFP Chromophore

method to compute excitation energy	method to optimize ground-state geometry	ΔE (eV)	wavelength (nm)	ref
INDO-CI	PM3	2.77	448	ref 18[a]
CIS/6-31G(d)	RHF/6-31G(d)	4.37	284	ref 20
TD-DFT(BP86)/6-31++G(d,p)	B3LYP/6-31++G(d,p)	2.94	421	ref 23[b]
CASPT2/6-31G(d)	CASSCF(12/11)/6-31G(d)	2.67	465	ref 22
SAC-CI/DZV	B3LYP/6-31G(d)	2.22	558	ref 21
MRMP2 based on SA-CASSCF (16/14)/(aug)-cc-pVDZ	PBE0/aug-cc-pVDZ	2.47	501	ref 24
aug-MCQDPT2 based on SA-CASSCF(16/14)/(aug)-cc-pVDZ	PBE0/aug-cc-pVDZ	2.54	489	ref 24
experiment		2.59	479	ref 14, 15

[a] A close value (444 nm) was obtained in the later semiempirical calculations of the NDDO type (ref 19). [b] For an overview of previous TD-DFT calculations using different functionals and basis sets, see Table 1 of ref 23; only the value closest to the experimental excitation energy is presented here.

multireference second-order Møller−Plesset perturbation theory (MRMP2)[45] and an extended version of the multiconfigurational quasidegenerate perturbation theory (aug-MCQDPT2)[46−48] (using ground-state equilibrium geometries optimized using DFT with the PBE0 functional[49,50] and the (aug)-cc-pVDZ basis set:[51] aug-cc-pVDZ on oxygen atoms and cc-pVDZ on all other atoms). The MRMP2 and aug-MCQDPT2 results are within 0.12 and only 0.05 eV from the experimental value, respectively (Table 1). These data suggest that one can compute the positions of absorption bands of biological chromophores with an accuracy of 10−20 nm (less than 0.1 eV) by applying perturbatively corrected CASSCF-based approaches. These techniques, however, are computationally demanding, and their execution requires advanced skills and extreme care, as the application of the method involves: (i) a careful selection of a large number of active space orbitals in fairly large basis sets; (ii) converging the state-averaged CASSCF solutions corresponding to the $\pi\pi^*$ transition, especially in realistic basis sets; and (iii) a careful and often ambiguous treatment of perturbative corrections to the reference CASSCF solutions. Moreover, gradient calculations are only available for bare CASSCF wave functions. Thus, it is desirable to find a more robust approach of a comparable accuracy for wider applications in modeling the properties of biological chromophores.

Contrarily to the bright singlet $\pi\pi^*$ state, little is known about the triplet states of the GFP chromophore. The fluorescence properties of GFP suggest that the intersystem crossing is not efficient, at least in the chromophore in the native protein environment. In the gas-phase photocycle, however, triplet states can play an important role. For example, possible population trapping in the triplet has been suggested as an explanation for observed millisecond-long lifetimes of the photoexcited ions in the ion storage ring experiments.[52] Spin-forbidden relaxation channels have also been considered in the studies of GFP mutants.[53,54]

In this work we discuss the character of the bright $\pi\pi^*$ state of the HBDI anion and continue to benchmark different perturbation theory corrected multiconfigurational approaches. We also apply the equation-of-motion coupled-cluster method with single and double excitations (EOM-CCSD)[55−60] as well as TD-DFT with the range-separated functionals, BNL[61] and ωPB97X.[62] We also characterize the lowest $\pi\pi^*$ triplet and report the vertical electron detachment energy (VDE). Based on the calculated VDE, we assign the minor feature as due to the photodetachment transition. This has important implications on the character of the bright state: the $\pi\pi^*$ transition is a resonance state embedded in the ionization continuum. The triplet state, however, lies below VDE. As a resonance state, the $\pi\pi^*$ singlet has a finite lifetime and can undergo autoionization due to coupling to the ionization continuum. Contrary to that, the triplet may have a much longer lifetime. Thus, population trapping in the triplet state in the gas-phase photocycle seems to be required to explain millisecond kinetics of the fragments yield in the ion storage ring experiments.[52] Moreover, the resonance nature of the $\pi\pi^*$ state in the anionic GFP might be responsible for very different kinetics of the photofragment yield of the anionic and protonated GFP.[52]

2. Computational Methods

The equilibrium geometries were optimized by DFT with the PBE0 variant[50] of the Perdew−Burke−Ernzerhof (PBE) hybrid functional[49] and by CASSCF(14/12). The cc-pVDZ basis set[51] was used in both calculations. After observing noticeable differences in vertical excitation energies computed using these two geometries, we reoptimized the equilibrium structure using MP2 with cc-pVTZ,[51] which yields very accurate structures for well-behaved closed-shell molecules.[63] MP2 calculations employed the resolution-of-the-identity (RI) technique. The CASSCF and PBE0 structures are C_1, whereas the RI-MP2 optimization produced a C_s minimum. The Cartesian coordinates of the optimized structures are given in the Supporting Materials.

Vertical excitation energies were computed by MRMP2, TD-DFT with the BNL and ωPB97X functionals, CIS, scaled opposite-spin CIS with perturbative doubles (SOS-CIS(D)), and EOM-CCSD for excitation energies (EOM-EE-CCSD). The VDE was computed at the CASSCF geometry as the energy of the Hartree−Fock HOMO (Koopmans' theorem) by EOM-CCSD for ionization potentials (EOM-IP-CCSD) and by using the BNL HOMO energy (as described below, this is equivalent to computing VDE as the difference between the total BNL energies of the anion and the neutral radical). The ωPB97X and B3LYP Koopmans' theorem and ΔE values are also given for comparison.

Each method is outlined below, and computational details are given in the Results Section. MRMP2 calculations were carried out with the PC GAMESS version[64] of the GAMESS(US) quantum chemistry package.[65] CIS, SOS-MP2, SOS-CIS(D), EOM-CCSD, and BNL calculations were performed with Q-Chem.[66]

2.1. Multireference Møller−Plesset Perturbation Theory (MRMP2). The MRMP2 model[45] is a special single-state case of multiconfigurational quasidegenerate second-order perturbation theory (MCQDPT2)[46] implemented in GAMESS(US)[65] and PC GAMESS.[64] The zeroth-order (reference) wave functions are state-averaged CASSCF wave functions (Ψ_α^{CAS}) for the target state α. The unperturbed Hamiltonian operator is a sum of one electron Fock-like operators in which the occupation numbers are replaced by the diagonal elements of the CASSCF density matrix. Beyond zeroth-order multiconfigurational functions, the complementary eigenfunctions of the complete active space configuration interaction Hamiltonian as well as the wave functions generated by one- and two-electron excitations from the reference functions (S-space), are considered via the perturbation theory. The second-order corrections to the energy are given by

$$E_\alpha^{(2)} = \sum_j \frac{\langle \Psi_\alpha^{CAS} | V | \Phi_j \rangle \langle \Phi_j V | \Psi_\alpha^{CAS} \rangle}{E_\alpha^0 - E_j^{(0)}} \quad (1)$$

where functions Φ_j belong to the S-space of uncontracted determinants. In a similar approach, CASPT2,[34] the S-space consists of the contracted configurations. Both MRMP2 and CASPT2, diagonalize-then-perturb methods, are widely used to calculate the excitation energies of organic chromophores. A comprehensive benchmark study[67] reports excellent agreement between zeroth-order-corrected CASPT2[68] and an accurate approximation to the coupled-cluster with singles, doubles, and triples method (CC3).[69,70] Similar accuracy is observed in the recent computational studies employing the MRMP2 methodology.[46−48]

2.2. Scaled Opposite-Spin MP2 and Scaled Opposite-Spin CIS(D). Spin-component-scaled MP2 (SCS-MP2) is a semiempirical approach based on scaling different spin contributions to the MP2 correction as proposed by Grimme:[71]

$$E_c \approx E_{c,\mathrm{SCS-MP2}} = p_{ss} E_{ss}^{(2)} + p_{os} E_{os}^{(2)} \quad (2)$$

The parallel-spin component $E_{ss}^{(2)}$ and the antiparallel-spin component $E_{os}^{(2)}$ are scaled to correct for their unbalanced contributions to the MP2 correlation energy. Empirically found optimal values of the coefficients are $p_{ss} = 1/3$ and $p_{os} = 6/5$. SCS-MP2 provides an improved description for many systems in which the ground state has a single reference character.

As the opposite-spin contribution is the major one, Jung et al.[72] further simplified the model by dropping the same-spin term altogether and scaling the opposite-spin contribution up. Along with the RI technique, SOS-MP2 offers a significant improvement in computational performance compared to the original MP2. The scaling coefficient − the only empirical parameters in the method − can be optimized for a wide variety of systems.[73]

In the same manner as SOS-MP2 is introduced for correcting the ground-state energy, SOS-CIS(D) is designed for excitation energies.[74] The computational scaling of SOS-CIS(D) is only $\mathcal{O}(N^4)$, which is a significant improvement over the $\mathcal{O}(N^5)$ scaling of CIS(D). The accuracy of SOS-CIS(D) is very similar to that of CIS(D) for valence states, whereas the performance for the Rydberg states is improved. Based on a set of over 40 various excited states in over 20 organic molecules, the mean signed error in the SOS-CIS(D) vertical excitation energy is 0.02 eV for valence states and −0.08 eV for Rydberg transitions. Limitations of SOS-MP2 and SOS-CIS(D) are the same as MP2 and CIS(D), respectively. For example, these methods fail when the ground-state wave function acquires a significant multiconfigurational character, as at a *cis-trans* isomerization transition state, and for excited states with doubly excited character. Open-shell (e.g., doublet) states can also cause difficulties due to spin contamination.

2.3. Long-Range-Corrected Density Functionals. In long-range-corrected functionals, a range-separated representation of the Coulomb operator[75,76] is used to mitigate the effects of the self-interaction error. The contribution from the short-range part is described by a local functional, whereas the long-range part is described using the exact Hartree−Fock exchange. The separation depends on a parameter γ. In the BNL approach,[61] γ is optimized for each system using Koopmans-like arguments: γ is adjusted such that the HOMO energy equals the difference between the total BNL energies of the $N1$ and N-electron systems. Initial benchmarks[61,77] demonstrated an encouraging performance for excited states and even such challenging systems as ionized dimers. In ωPB97X,[62] γ and other parameters are optimized using standard training sets. Benchmark results have demonstrated consistently improved performance relative to uncorrected functionals.

2.4. Equation-of-Motion Coupled-Cluster Methods for Excitation Energies and Ionization Potentials. In EOM-CC,[55−60,78−80] the Hamiltonian is similarity transformed:

$$\bar{H} \equiv \exp(-T) H \exp(T) \quad (3)$$

using the cluster operator T obtained from coupled-cluster equations for the ground state:

$$\langle \Phi_\mu | \bar{H} - E^{CC} | \Phi_0 \rangle = 0 \quad (4)$$

where $|\Phi_\mu\rangle$ denotes all μ-tuply excited determinants with respect to the Hartree−Fock reference $|\Phi_0\rangle$. The solution for the m-th excited state is found from

$$\langle \Phi_\mu | \bar{H} - E_m^{EOM} | R_m \Phi_0 \rangle = 0 \quad (5)$$

where R_m is a linear excitation operator, the form of which depends on the target states. For example, in equation-of-motion for excitation energies (EOM-EE) R_m is

$$R_m = r_{m,0} + \sum_{ia} r_{m,i}^a a^\dagger i + \frac{1}{4} \sum_{ijab} r_{m,ij}^{ab} a^\dagger b^\dagger j i + \ldots \quad (6)$$

whereas for ionized states, R_m is not particle conserving

$$R_m = \sum_i r_{m,i} i + \frac{1}{4} \sum_{ija} r^a_{m,ij} a^\dagger j i + \ldots \quad (7)$$

The EOM wave function of the m-th state is given by

$$|\Psi_m\rangle = R_m \exp(T)|\Phi_0\rangle \quad (8)$$

In EOM-CCSD, the excitation operator R_m is truncated after the two-body term (i.e., two-hole two-particle for EE and two-hole one-particle for IP), and the similarity transformed Hamiltonian is diagonalized in the basis of all singly and doubly excited determinants.

The EOM-CCSD error bars are 0.1−0.3 eV for electronic states dominated by a single excitation. Including triples reduces the error to 0.01−0.02 eV.[81] In a recent benchmark study, Schreiber et al.[67] reported EOM-CCSD mean absolute and maximum errors of 0.12 and 0.23 eV, respectively. A recent study of uracil[82] demonstrated that even for well-behaved molecules inclusion of triple excitations and extending the basis set beyond augmented double-ζ can affect vertical excitations by as much as 0.3 eV.

3. Results and Discussion

3.1. Molecular Orbital Framework. Figure 2 shows two resonance structures of the HBDI anion. The interaction between these two structures results in charge delocalization between the two oxygen atoms and in scrambling CC bond orders, as discussed for example in ref 42. Changes in bond orders in the bridge region due to the resonance are believed to be important in thermal isomerization,[83] as discussed in detail in the companion paper.[12]

The natural bond orbital (NBO)[84,85] charges on the phenoxy or imidazolin oxygens (computed using the RI-MP2 densities) are −0.65 and −0.66, respectively. The almost equal values of the charges suggest significant contributions from both resonance structures. As the result of the resonance interaction, the C_{1P}−C_{1B} bond gains double-bond character, whereas the order of C_{1B}−C_{1I} bond is reduced, and the bridge moiety acquires allylic character. It is interesting to compare the respective bond lengths with the values for the double and single CC bonds between sp^2 hybridized carbons, e.g., in a planar and twisted ethylene (see ref 86 for explanation regarding the choice of the reference structures). Our best estimates of the C_{1P}−C_{1B} and C_{1B}−C_{1I} bond lengths (RI-MP2/cc-pVTZ) are 1.394 and 1.378 Å, respectively. The lengths of the CC bond in ethylene is 1.333 Å at the planar geometry (where the formal bond order is 2) and 1.470 Å[87] at the twisted configuration, where the π bond is completely broken.[86] Thus, assuming a linear relationship between the bond order and bond length, one can assign 55 and 67% of a double-bond character to the C_{1P}−C_{1B} and C_{1B}−C_{1I} bonds, respectively. The NBO analysis[84,85] assigns 1.8 electrons to a slightly asymmetric allylic three-center bond. The relative contributions of the C_{1P} and C_{1I} carbons are 38 and 62%, respectively, in a semiquantitative agreement with the bond orders derived from the bond lengths.

The resonance interaction is also reflected by the shape of MOs. Figure 3 shows two Hartree−Fock orbitals involved in the bright $\pi\pi^*$ and the photodetachment transitions (HOMO and valence LUMO). These orbitals, which are traditionally referred to as π and π^*, have quite complicated shapes and are delocalized over the entire molecule. Their character in the bridge region can be explained by considering two interacting π orbitals, as shown in Figure 3. The HOMO can be described as an out-of-phase combination of two localized π bonds, whereas the large electron density on C_{1B} in the LUMO can be derived from the in-phase combination. Of course, due to the delocalized character of the orbitals, this picture is just an approximation, but it allows one to see the origin of the large oscillator strengths and changes in charge distribution in the excited state and also provides a useful framework for explaining the character of the transition state along the *cis-trans* isomerization coordinate.[12]

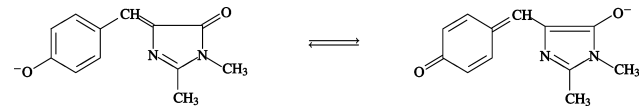

Figure 2. Two resonance structures of the HBDI anion.

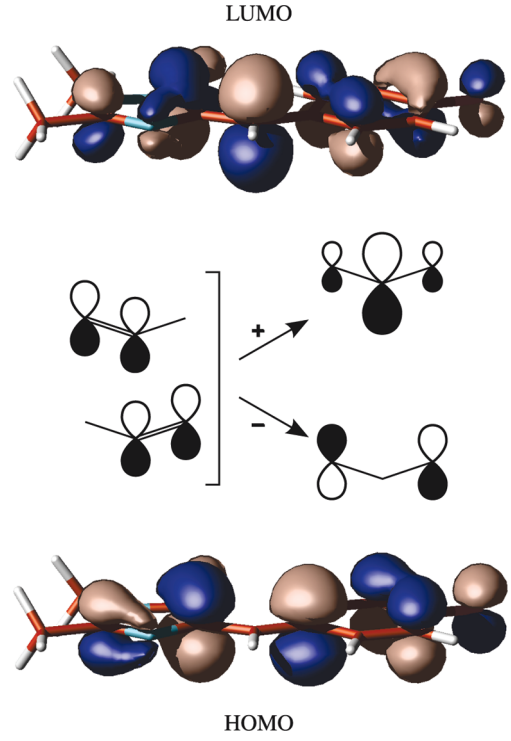

Figure 3. Two molecular orbitals of the HBDI anion giving rise to the $\pi\pi^*$ state. The character of the orbitals can be explained by considering the linear combination of two localized π-bonding orbitals.

3.2. Vertical Electron Detachment Energy of the HDBI Anion. Since the HBDI anion is a closed-shell system, it is stable in the gas phase and has a relatively large VDE. However, as shown below, it does not support bound electronically excited singlet states, and the lowest valence excitation is embedded in an ionization continuum. Such resonance states are very common in molecular anions[88] and play an important role in dissociative electron attachment processes.[89,90] Thus, the broad character of the experimental action spectrum[14,15] is at least partially due to the broadening of the resonance-like $\pi\pi^*$ state by its interaction with the ionization continuum. Finite lifetime and autoionization

decay of this state should be taken into account when considering photoinduced dynamics and lifetime of the HBDI anion in the gas phase. In the condensed phase, solvent may stabilize the anion such that its excited states become bound. However, one photon photodetachment channel may still be relevant for the anionic forms, especially when the production of solvated electrons is considered.[91] The resonance character of the $\pi\pi^*$ state also has significant consequences in the electronic structure calculations[59,88] of excited states, as described below.

The simplest estimate of VDE obtained by applying Koopmans' theorem is 2.56−2.93 eV depending on the basis set, the largest value obtained with the 6-311(2+,+)G(2df,2pd) basis. The EOM method for ionization energies (EOM-IP), which includes electronic correlation, can provide more reliable estimates of VDE. However, due to the size of the system, we are limited to relatively modest basis sets. In the 6-31G* basis, Koopmans' VDE is 2.56 eV, while EOM-IP-CCSD yields 2.05 eV. The larger 6-31+G* basis increases the energies to 2.91 and 2.48 eV, respectively. Thus, including correlation reduces VDE by 0.4−0.5 eV and assuming the effect is consistent throughout basis sets, we estimate that the target EOM-IP-CCSD/6-311(2+,+)-G(2df,2pd) energy is 2.4−2.5 eV.

B3LYP/cc-pVDZ energy difference calculations yield 2.46 eV, which is considerably larger than the respective Koopmans value of 0.92 eV. The ωPB97X/cc-pVDZ energy difference value is 2.39 eV, whereas the respective Koopmans IE is much higher (2.83 eV).

By construction, the BNL energy difference VDE is equal to the respective HOMO energy. Recent benchmarks[92] demonstrated that BNL produces very accurate ionization energies. VDE calculated with BNL in the small cc-pVDZ basis is 1.99 eV ($\gamma = 0.250$), and it increases to 2.52 eV in the 6-311G(2+,+)G(d,p) basis for which $\gamma = 0.228$. Additional sets of diffuse orbitals or more extensive polarization do not affect this value, e.g., VDE calculated with BNL/6-311G(3+,2+)G(2df,2pd) is 2.53 eV.

The discrepancies between the Koopmans and ΔE values have important implications for the excited-state calculations, as the former value defines the onset of the ionization continuum in CIS/TD-DFT calculations (see Appendix). Thus, with B3LYP, the continuum begins 1.54 eV below its own VDE, whereas the situation with ωPB97X is reverse, i.e., the continuum states appear 0.44 eV above the respective VDE. BNL, by constriction, is internally consistent, and the continuum states in TD-DFT calculations appear exactly at the respective VDE.

Thus, our estimate of VDE is 2.4−2.5 eV, within 0.1 eV from the maximum of the weak absorption feature at 2.3 eV. The remaining discrepancy between the two values might be due to the uncertainties in equilibrium geometries or possible vibrational excitation of the molecules in the experiment.

Although correlation has significant effect on VDE, the ionized state has Koopmans-like character, i.e., the leading EOM-IP amplitude corresponds to ionization from the HOMO (see Figure 3) and equals 0.96. Thus, the Hartree−Fock HOMO is a good approximation to a correlated Dyson orbital.[93]

3.3. Vertical Excitation Energy and Electronic Properties of the Singlet and Triplet $\pi\pi^*$ Transitions of the HBDI Anion. *3.3.1. Singlet $\pi\pi^*$ State: Benchmark Results.* Motivated by the discrepancies in previous theoretical estimates of the $\pi\pi^*$ excitation energy of the HBDI anion (Table 1), we set out to benchmark other electronic structure methods with the purpose of identifying a rigorous, yet fairly inexpensive, quantum chemistry approach that can be employed in condensed-phase applications. The experimental maximum of absorption is at 2.59 eV (479 nm), and the band's full width at half-maximum (fwhm) is 0.25 eV (45 nm).[14,15] Assuming that the absorption maximum corresponds to the vertical transition of the lowest-energy isomer (which is not entirely clear, as the temperature of the ions in the ring is unknown), one would like the computed wavelength to fall within 2.47−2.72 eV (456−502 nm). However, due to the resonance nature of the $\pi\pi^*$ state, calculating the excitation energies and oscillator strengths, as well as comparing them with the experimental spectrum, are not as straightforward as in the case of the excited states lying below the electron detachment energy. In the following, we will use the term "detached states" to identify the electronic states that compose the continuum instead of the usual "ionized states" as the initial species is anionic.

The ground-state equilibrium geometry was optimized with PBE0/cc-pVDZ, CASSCF/cc-pVDZ, and RI-MP2/cc-pVTZ (see Computational Methods section). Although the differences between the geometries are small (maximum bond length deviation is 0.03 Å and angles agree within 2 degrees), the $\pi\pi^*$ excitation energy computed using wave function-based methods differs by about 0.1 eV. This effect of geometry is consistent with previous calculations by Olsen[94] for a similar system (*p*-hydroxybenzylidene-imidazolin-5-one, HBI). Of the three structures, the RI-MP2/cc-pVTZ is the most accurate.[63] Since most of the changes in electron density occur in the bridge region, it is interesting to compare the $C_{1P}-C_{1B}$ and $C_{1B}-C_{1I}$ bond lengths computed by different methods. The RI-MP2 values are 1.394 and 1.378 Å, which is very close to the PBE0 values of 1.404 and 1.385 Å. Due to the absence of dynamical correlation, CASSCF exaggerates the bond alternation giving 1.406 and 1.397 Å.

Calculations in small basis sets create discrete states from the continuum and artificially exclude the detached states from the picture. Assuming that the character of the resonance state of interest is well described, such calculations may provide a fairly good estimate of the position of this state in the continuum, however, it is difficult to predict how expanding the basis set will affect the resonance state.[59,88] Moreover, one should anticipate broadening of the resonance state due to the interaction with the detached states. Increasing the size of the one-electron basis brings the continuum states down. When the basis set is large enough to accommodate a detached electron, the lowest excited state will correspond to the detached state (this fact has been exploited in pilot implementations of EOM-IP-CCSD based on the EOM-EE-CCSD code by adding a very diffuse orbital to the basis to describe the ionized electron).[95,96] It can be shown formally (see Appendix) that, in the case of CIS and

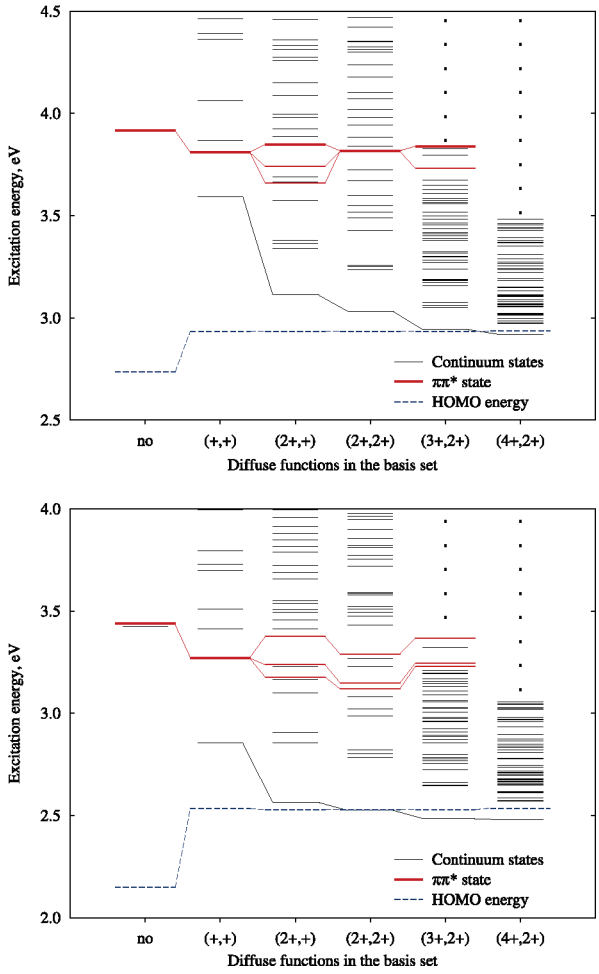

Figure 4. Effect of increasing the number of diffuse functions in the basis set on the density of states and the convergence of the lowest excited and the bright $\pi\pi^*$ state. The calculations were performed with CIS (top) and TD-DFT/BNL (bottom). The basis set was varied from 6-311G(2pd,2df) to 6-311-(4+,2+)G(2pd,2df).

TD-DFT, the energy of the lowest of such CIS-IP states equals the HOMO energy, that is, the Koopmans theorem can be proven by considering the configuration interaction of all singly detached determinants.

When the one-electron basis set is expanded with diffuse functions, the density of states rapidly increases with both CIS and TD-DFT (BNL), as illustrated in Figure 4. At the same time, the lowest excited state converges to Koopmans' VDE. Both methods split the oscillator strength of the bright $\pi\pi^*$ transition among multiple states, but BNL does that to a larger degree, which results in three to four states with close oscillator strengths (Table 2). That may be due to the remaining self-interaction error in BNL calculations.

Seemingly in contradiction with the proof given in the Appendix, the lowest excited CIS and TD-DFT states shown in Figure 2 fall below the Koopmans estimate in large basis sets due to additional stabilization by the interaction with other CIS determinants that vanish once the detached electron is infinitely far from the core. Indeed, if a separate large noninteracting orbital is used instead of diffuse functions, the lowest excitation energy in such a system is exactly equal to the HOMO energy.

Table 2. Interaction of the Bright $\pi\pi^*$ State with the Electron Detached Continuum as Reflected by the Diminishing Oscillator Strength (f_L) in CIS and TD-DFT/BNL Calculations[a]

basis set	number	energy, eV	f_L
	CIS		
6-311G(2df,2pd)	1	3.92	1.58
6-311(+,+)G(2df,2pd)	2	3.81	1.50
6-311(2+,+)G(2df,2pd)	6	3.66	0.22
	9	3.74	0.14
	10	3.85	1.14
6-311(2+,2+)G(2df,2pd)	9	3.60	0.08
	12	3.82	1.35
	17	4.02	0.06
6-311(3+,2+)G(2df,2pd)	37	3.73	0.43
	40	3.84	1.00
	TD-DFT (BNL)		
6-311G(2df,2pd)	2	3.44	1.47
6-311(+,+)G(2df,2pd)	3	3.27	1.38
6-311(2+,+)G(2df,2pd)	7	3.18	0.54
	9	3.24	0.31
	10	3.38	0.52
6-311(2+,2+)G(2df,2pd)	8	3.12	0.15
	9	3.15	0.15
	12	3.29	0.39
	13	3.29	0.63
6-311(3+,2+)G(2df,2pd)	35	3.23	0.47
	37	3.24	0.39
	39	3.37	0.15
	40	3.37	0.15

[a] Also see Fig 4.

As the density of low-lying states that approximate the continuum increases and the oscillator strength gets redistributed, it becomes increasingly more difficult to compute or even identify the resonance state. By following the evolution of the states with the basis set increase, the limiting value of the resonance state can be extrapolated using the stabilization method by Taylor,[97] as has been done in the calculations of resonance electron attached states.[59,88] From the data in Table 2, we can estimate that the excitation energy converges to 3.8 eV with CIS and to 3.3 eV with TD-DFT/BNL. Overall, adding sets of diffuse functions results in lowering the excitation energy of the bright state by 0.1 eV.

The CIS and TD-DFT/BNL calculations demonstrate that the resonance state is embedded in an electron detached continuum, and the broad character of the experimental spectrum can be due to the interaction with the continuum. Thus, small basis set calculations of the vertical excitations energies of the $\pi\pi^*$ state can only provide a rough estimate of the position of the absorption maximum.

Introducing a noniterative doubles correction via SOS-CIS(D) significantly lowers the energy of the $\pi\pi^*$ transition, while the detached state energies are affected less. We could not obtain SOS-CIS(D) results in heavily augmented basis sets due to the lack of the corresponding auxiliary bases for the RI procedure, which becomes unstable upon adding a second set of the diffuse functions. The magnitude of correction is 0.9−1.2 eV for the $\pi\pi^*$ state and 0.1−0.3 eV for the detached states. MRMP2 based on sa-CASSCF(14/12) in the modest cc-pVDZ basis yields 2.51−2.61 eV for the $\pi\pi^*$ excitation energy. SOS-CIS(D)/cc-pVDZ gives 2.71−2.81 eV, which is consistent with the more rigorous MRMP2 estimates.

Table 3. Vertical $\pi\pi^*$ Electronic Excitation Energies (ΔE, in eV), Corresponding Wavelengths (nm), and Oscillator Strength (f_L) for the Gas-Phase GFP Chromophore (Figure *1*)[d]

	Ground-state geometry optimized with								
	PBE0/cc-pVDZ			CASSCF(14/12)/cc-pVDZ			RI-MP2/cc-pVTZ		
Method	ΔE	f_L	nm	ΔE	f_L	nm	ΔE	f_L	nm
MRMP2 based on sa-CASSCF(14/12)/cc-pVDZ	2.52[b]	–	491[b]	2.61[c]	–	476[c]	–	–	–
EOM-CCSD/6-31G(d)	3.08	1.26	402	3.16	1.27	392	3.12	1.27	398
EOM-CCSD/6-31+G(d)	2.97	1.24	418	3.04	1.25	408	3.00	1.25	413
SOS-CIS(D)/cc-pVDZ	2.71	1.59[a]	457	2.81	1.61[a]	441	2.75	1.60[a]	451
SOS-CIS(D)/aug-cc-pVDZ	2.57	1.45[a]	482	2.67	1.45[a]	464	2.61	1.45[a]	475
SOS-CIS(D)/cc-pVTZ	2.58	1.54[a]	480	2.68	1.56[a]	463	2.62	1.54[a]	473
SOS-CIS(D)/aug-cc-pVTZ	2.58	1.37[a]	480	2.90	1.04[a]	427	2.72	1.23[a]	456
TD-DFT/BNL/cc-pVDZ	3.44	1.51	360	3.50	1.51	354	3.59	1.55	346
TD-DFT/BNL/6-311(+,+)G(2df,2pd)	3.22	1.38	385	3.27	1.38	379	3.24	1.38	383
TD-DFT/ωPB97x/cc-pVDZ	3.52	1.52	352	3.59	1.53	346	3.55	1.53	349
TD-DFT/ωPB97x/6-311(+,+)G(2df,2pd)	3.38	1.45	367	3.44	1.46	360	3.40	1.45	364

[a] Oscillator strength calculated with CIS. [b] At the equilibrium geometry computed with PBE0/(aug)-cc-pVDZ (diffuse functions only on oxygen atoms). [c] At the equilibrium geometry computed with CASSCF(12/11)/(aug)-cc-pVDZ (diffuse functions only on oxygen atoms). [d] The reference experimental value is 2.59 eV (479 nm) (ref 14, 15).

At the CASSCF optimized geometry, EOM-CCSD/6-31G* yields an excitation energy of 3.16 eV and an oscillator strength $f_L = 1.27$. Including only one set of diffuse functions lowers the energy to 3.04 eV ($f_L = 1.25$). The change in the oscillator strength is consistent with the observed drop of the EOM amplitude corresponding to the $\pi\pi^*$ transition from 0.85 to 0.74. Benchmarks on the electronically excited states of closed-shell molecules have shown that the combined effect of increasing the basis set in EOM-CCSD calculations and the triples correction can be as large as 0.3−0.4 eV.

The computational cost of MRMP2 and EOM-CCSD does not allow us to use these methods to fully explore the basis set effect on the $\pi\pi^*$ excitation energy, e.g., via stabilization method. We anticipate a noticeable effect of improving the basis set on the energy of the $\pi\pi^*$ state. For example, with SOS-CIS(D), the excitation energy with the cc-pVTZ basis is lower by 0.13 eV relative to cc-pVDZ. The EOM-CCSD excitation energy also drops by as much as 0.2 eV upon expanding the basis set from 6-31G* to 6-31+G*. The oscillator strength calculated with CIS is about 10% lower when basis sets with diffuse functions are used compared to those without, demonstrating the beginning of the interactions with the continuum.

The $\pi\pi^*$ excitation energy obtained with MRMP2 based on state-averaged CASSCF(16/14), which spans the entire π-electron active space (Table 1), and a more compact (14/12) active space (Table 3) agree equally well with the experimental result: 2.47 eV (501 nm) and 2.52−2.61 eV (476−491 nm), respectively, versus 2.59 eV (479 nm). The most expensive aug-MCQDPT2/CASSCF(16/14) approach (Table 1) does not perform noticeably different than MRMP2/CASSCF(14/12). Therefore, one can rely on the fairly practical MRMP2 approach based on a reduced active space in the CASSCF wave function. Overall, the effect of contracting the active space is less than 0.1 eV, which is smaller than the uncertainty due to the equilibrium geometry and anticipated effects of extending the basis set beyond the double-ζ level.

In view of complexities associated with performing multireference perturbation theory and underlying CASSCF calculations, we find the results of the inexpensive SOS-CIS(D) method very encouraging: at the PBE0-optimized geometry, the SOS-CIS(D)/cc-pVTZ $\pi\pi^*$ excitation energy of 2.58 eV is within 0.01 eV from the experimental absorption maximum and agrees very well with MRMP2 calculations.

The EOM-CCSD/6-31+G* excitation energy is 0.38 eV above the experimental maximum, which is outside the EOM-CCSD error bars. Analysis of the EOM amplitudes confirms a singly excited character of the $\pi\pi^*$ state, thus, with an adequate basis set, EOM-CCSD error should not exceed 0.3 eV. In addition to anticipated basis set effects and interactions with the continuum states, other factors, such as discrepancies due to equilibrium geometry as well as the uncertainty in the experimental value (fwhm of the experimental absorption is 0.25 eV), make it difficult to arrive at a definite conclusion. More extensive calculations using larger basis sets (and ideally using stabilization graphs) and estimates of triples corrections (to account for dynamical correlation) are required to assess the performance of EOM-CCSD for this molecule. Basis set and triples effects alone have been shown to account for as much as 0.3 eV in excitation energies of $\pi\pi^*$ character.[82]

Finally, we present TD-DFT results computed with the range-separated functionals. Using the BNL functional[61] with the small cc-pVDZ basis set, the $\pi\pi^*$ state appears the second lowest, which is consistent with the respective VDE. At the CASSCF geometry, its excitation energy is 3.50 eV, and the oscillator strength is $f_L = 1.51$. The 6-311(+,+)G(2df,2pd) basis lowers the excitation energy to 3.27 eV, and the oscillator strength to 1.38. ωPB97X[62] gives similar values for the excitation energy and the

Table 4. Vertical Triplet $\pi\pi^*$ Electronic Excitation Energies (ΔE, in eV) of the HBDI Anion in the Gas Phase

basis set	CIS	SOS-CIS(D)
cc-pVDZ	2.03	1.91
aug-cc-pVDZ	2.02	1.88
cc-pVTZ	2.03	1.86

oscillator strengths, i.e., 3.59 ($f_L = 1.51$) and 3.44 eV ($f_L = 1.46$) with cc-pVDZ and 6-311(+,+)G(2df,2pd), respectively. Because the Koopmans continuum with ωPB97X begins at higher energies (see Section 3.2, Vertical Electron Detachment Energy of the HDBI Anion), the detached states do not appear below the excited states in these calculations.

Overall, it is unrealistic to expect accuracy better than 0.1 eV (20 nm) from computational protocols applicable to a molecule of this size even for nonresonance states, and the observed discrepancies between different methods confirm that. Moreover, when assessing the accuracy of computed values, one should keep in mind the finite width of the experimental absorption band. Thus, more calculations are necessary to provide a converged theoretical estimate, especially stabilization analysis. For practical applications, however, it is important that all the reliable theoretical methods agree with each other in that the origin of the intensity in the resonance state is due to $\pi\pi^*$ excitation. SOS-CIS(D) offers an inexpensive alternative to more rigorous multireference methods if single excitations are dominant in the wave function.

3.3.2. Changes in Electronic Density in the Singlet $\pi\pi^*$ State. As one may expect from the molecular orbital character (Figure 3) and the large oscillator strength, electronic excitation results in a significant redistribution of electronic density. A convenient measure of charge distribution is the permanent dipole moment. Although in a charged system it is origin dependent, the difference between the two dipole moments, $\Delta\mu = \mu_{gr} - \mu_{ex}$, is not. At the CIS level of theory, the value of $|\Delta\mu|$ is 0.6 D, and its direction is in the molecular plain pointing toward the bridge carbon. This value can be compared with the experimentally measured $\Delta\mu$, derived from Stark effect measurements in a buffered (pH = 6.5) glycerol solution at 77 K.[17] This work also reports the angle between $\Delta\mu$ and $\Delta\mu_{tr}$. Strikingly, the experimental value is 10 times larger than the computed one. Since $\Delta\mu$ is related to the changes in orbital occupations upon excitation, it is dominated by contributions from the leading excitation amplitudes and should be reproduced fairly accurately at the CIS level. Thus, large discrepancy is likely to be due to the solvent effect. Indeed, polar solvents result in the increased dipole moment of the solute. For example, the dipole moment of water in bulk water is about 30% larger than in the gas phase. More polar charge distribution in the ground state in solvent is clearly seen from the respective NBO charges (see Table 2 in ref 12). Thus, for the difference of dipole moments of two states, one may anticipate an enhanced effect.

3.3.3. Triplet $\pi\pi^*$ State. The vertical excitation energies of the lowest triplet state at the RI-MP2/cc-pVTZ geometry are summarized in Table 4. The analysis of the wave function confirms that the triplet is derived from the transitions between the same orbitals as the singlet (Figure 3). As expected, all methods consistently place the triplet considerably below the singlet. The variations between the methods are smaller for the triplet state. Our best value (SOS-CIS(D)/cc-pVTZ) is 1.86 eV. The 0.76 eV gap between the singlet and triplet does not suggest efficient intersystem crossing at this geometry. The triplet state is 0.3−0.4 eV below VDE and is, therefore, a bound electronic state. Thus, much longer lifetime is expected for this state (as compared to the singlet), not only because the radiationless relaxation to the ground state is a spin-forbidden process, but also because the autoionization channel is absent.

4. Conclusions

In this work we exploit modern quantum chemical methods for calculations of the electronic properties of the GFP chromophore and compare the results to the gas-phase absorption spectrum obtained by photodestruction spectroscopy in the ion storage ring.[14,15,52]

The experimental action spectrum of the denatured gas-phase anionic GFP chromophore features a broad line (2.4−2.8 eV) with a maximum at 2.59 eV and a minor feature at 2.3 eV. Wave function-based and DFT calculations estimate a VDE of 2.4−2.5 eV. Thus, we assign the minor peak as due to the photodetachment transition. Based on our estimate of VDE, the absorption band at 2.6 eV corresponds to the transition to the resonance state embedded in an electron detached continuum, and the broad character of the spectrum is at least partially due to the interaction with the continuum states.

The resonance nature of the $\pi\pi^*$ state suggests a finite lifetime, and that autoionization channel should be considered when modeling the anionic GFP photocycle. The triplet state is found to be well below the photodetachment threshold (vertical excitation energy 1.86 eV). Thus, the two states are expected to have very different lifetimes, which makes the suggested[52] population trapping in the triplet state even more essential for explaining slow fragmentation kinetics. The resonance nature of the $\pi\pi^*$ state in the anionic GFP might be responsible for very different behavior of the photofragment yield of the anionic and protonated GFP,[52] however, more detailed electronic structure calculations are required in order to suggest a viable mechanism. An important question is how photoinduced isomerization and other structural changes[42,98] affect the relative-states energies.

All wave function-based and TD-DFT methods agree on the nature of the transition lending the intensity to the resonance state, which is a bright $\pi\pi^*$ transition (HOMO−LUMO in a small basis set), however, quantitative agreement is more difficult to achieve. Most importantly, small basis set calculations discretize the ionization continuum, and the results of such calculations provide only a crude estimate of the energy of the resonance state. In order to account for basis set effects, the stabilization analysis can be used; however, in view of the large size of the GFP chromophore molecule, we were able to only conduct it with the CIS and BNL methods.

Nevertheless, it is instructive to compare vertical excitation energies of the $\pi\pi^*$ state computed with different methods

in a moderate basis set and with the experimental band maximum. While the CIS/aug-cc-pVTZ excitation energy is more than 1 eV off, perturbative inclusion of double excitations by SOS-CIS(D) yields a value which is within 0.1 eV from the experimental band maximum. The EOM-CCSD values computed in the modest 6-31+G* basis are within 0.38 eV from the experimental absorption maximum. An analysis of the EOM-CCSD wave function confirms the dominant one electron character of the $\pi\pi^*$ state, however, perturbative inclusion of triple excitations and a larger basis set are required for a converged (with respect to the level of theory) EOM-CC value. Based on previous studies, a proper account of dynamical correlation by including triple excitations and increasing basis set can change the vertical excitation energy by as much as 0.3 eV. Basis set effects evaluated using inexpensive SOS-CIS(D) calculations affect vertical excitation energies by 0.14 eV upon the transition from cc-pVDZ to aug-cc-VTZ.

Additional uncertainties arise from the ground-state geometry. For example, different choices of the ground-state geometry (optimized with CASSCF, DFT, and MP2) introduce an uncertainty of 0.1 eV in the vertical excitation energies. A relatively strong dependence of the excitation energy on the structure suggests additional broadening of the absorption band due to vibrational excitations of the chromophore.

The best MRMP2 estimate is within 0.07 eV from the experimental band maximum, however, the inclusion of basis set effects (using the SOS-CIS(D)/aug-cc-pVTZ estimate) increases the difference to 0.21 eV. Overall, the observed variations demonstrate that it is unrealistic to expect an accuracy better than 0.1 eV from computational protocols applicable to a molecule of this size even for nonresonance excited states.

BNL/cc-pVDZ vertical excitation energy of the bright $\pi\pi^*$ transition is above MRMP2/cc-pVDZ value by 0.9 eV. Since the self-interaction error is considerably reduced in BNL, the photodetachment continuum is likely not contaminated by spurious low-lying charge-transfer states ubiquitous in TD-DFT calculations.

Acknowledgment. We thank Alex Granovsky and Dr. Ksenia Bravaya for their generous help and valuable discussions of this work. This work is supported by the joint grant from the U.S. Civilian Research and Development Foundation (project RUC1-2914-MO-07) and the Russian Foundation for Basic Research (08-03-91104-AFGIR). I.P., B.G., and A.N. thank the SKIF-GRID program and SKIF-Siberia for providing computational resources. E.E. and A.I.K. thank Prof. Roi Baer and Dr. Esti Livshitz for their help with performing BNL calculations. E.E. and A.I.K. acknowledge the iOpenShell Center for Computational Studies of Electronic Structure and Spectroscopy of Open-Shell and Electronically Excited Species (http://iopenshell.usc.edu) supported by the National Science Foundation through the CRIF:CRF CHE-0625419 + 0624602 + 0625237 grant as well as through the CHE-0616271 grant (A.I.K.). A.I.K. is grateful to the Institute of Mathematics and its Applications in Minnesota for its hospitality and productive environment during her stay at IMA as a visiting professor. We also wish to thank the reviewer of the manuscript for his/her thoughtful and insightful comments.

Supporting Information Available: Optimized geometry of the HBDI anion, CASSCF natural orbital figures, and leading EOM-CCSD amplitudes additional information. This material is available free of charge via the Internet at http://pubs.acs.org.

Appendix

The electronic Hamiltonian in the second quantization form is

$$H = \sum_{pq} \langle p|h|q\rangle p^\dagger q + \frac{1}{2}\sum_{pqrs} \langle pq|rs\rangle p^\dagger q^\dagger sr \qquad (9)$$

where h is the core Hamiltonian operator, $\langle pq|rs\rangle$ denotes two electron integrals, and the sums run over all the MOs.

The choice of the reference determinant $|\Phi_0\rangle$ defines the separation of the orbital space into the occupied and virtual subspaces. Let $\{i,j,...\}$ be the subspace of all occupied and $\{a,b,...\}$ be the subspace of all virtual orbitals in $|\Phi_0\rangle$. Indexes $p,q,...$ denote all orbitals, occupied or virtual.

Let $|\Phi_0\rangle$ be the solution to the Hartree−Fock equations with an energy value:

$$E_0 = \langle\Phi_0|H|\Phi_0\rangle = \sum_i \langle i|h|i\rangle + \frac{1}{2}\sum_{ij}\langle ij||ij\rangle \qquad (10)$$

$|\Phi_n\rangle$ is the determinant derived by removing an electron from orbital n of $|\Phi_0\rangle$: $|\Phi_n\rangle = n|\Phi_0\rangle$, $\langle\Phi_m| = \langle\Phi_0|m^\dagger$. The Hamiltonian matrix element between two ionized determinants is

$$\langle\Phi_m|H|\Phi_n\rangle = \sum_{pq}\langle\Phi_0|m^\dagger p^\dagger qn|\Phi_0\rangle\langle p|h|q\rangle + \frac{1}{2}\sum_{pqrs}\langle\Phi_0|m^\dagger p^\dagger q^\dagger srn|\Phi_0\rangle\langle pq|rs\rangle \qquad (11)$$

Using the anticommutation relation $pq^\dagger + q^\dagger p = \delta_{pq}$, it is not difficult to show that

$$\sum_{pq}\langle\Phi_0|m^\dagger p^\dagger qn|\Phi_0\rangle = \sum_i \langle i|h|i\rangle\delta_{mn} - \langle n|h|m\rangle \qquad (12)$$

$$\frac{1}{2}\sum_{pqrs}\langle\Phi_0|m^\dagger p^\dagger q^\dagger srn|\Phi_0\rangle\langle pq|rs\rangle = \frac{1}{2}\sum_{ij}\langle ij||ij\rangle\delta_{mn} - \sum_j\langle nj||mj\rangle \qquad (13)$$

$$\langle\Phi_m|H|\Phi_n\rangle = \delta_{mn}\left(\sum_i\langle i|h|i\rangle + \frac{1}{2}\sum_{ij}\langle ij||ij\rangle\right) - \langle n|h|m\rangle - \sum_j\langle nj||mj\rangle = \delta_{mn}E_0 - \langle n|f|m\rangle \qquad (14)$$

Since the Fock matrix f is diagonal in the basis of Hartree−Fock orbitals, the matrix element becomes

$$\langle\Phi_m|H|\Phi_n\rangle = (E_0 - \varepsilon_n)\delta_{mn} \qquad (15)$$

where $\varepsilon_n = \langle n|h|n\rangle + \sum_j \langle nj||nj\rangle$ is a diagonal Fock matrix element and the energy of the n-th Hartee−Fock orbital.

Therefore, the Hamiltonian is diagonal in the basis of the electron detached or ionized determinants. The excitation energies of such states are equal to the respective orbital energies. Thus, configuration interaction of singly detached state functions is equivalent to Koopmans' theorem. This provides a useful diagnostic for TD-DFT: spurious states will appear in large bases at the onset of Koopmans continuum, i.e., HOMO energy.

References

(1) Tsien, R. Y. *Annu. Rev. Biochem.* **1998**, *67*, 509.

(2) Zimmer, M. *Chem. Rev.* **2002**, *102*, 759.

(3) Stepanenko, O. V.; Verkhusha, V. V.; Kuznetsova, I. M.; Uversky, V. N.; Turoverov, K. K. *Curr. Protein Pept. Sci.* **2008**, *9*, 338.

(4) Chen, R. F. *Arch. Biochem. Biophys.* **1977**, *179*, 672.

(5) Steiner, R. F.; Albaugh, S.; Nenortas, E.; Norris, L. *Biopolymers* **1997**, *32*, 73.

(6) Babendure, J. R.; Adams, S. R.; Tsien, R. Y. *J. Am. Chem. Soc.* **2003**, *125*, 14716.

(7) Silva, G. L.; Ediz, V.; Yaron, D.; Armitage, B. A. *J. Am. Chem. Soc.* **2007**, *129*, 5710.

(8) Constantin, T. P.; Silva, G. L.; Robertson, K. L.; Hamilton, T. P.; Fague, K.; Waggoner, A. S.; Armitage, B. A. *Org. Lett.* **2008**, *10*, 1561.

(9) Özhalici-Ünal, H.; Pow, C. L.; Marks, S. A.; Jesper, L. D.; Silva, G. L.; Shank, N. I.; Jones, E. W.; Burnette, J. M.; Berget, P. B.; Armitage, B. A. *J. Am. Chem. Soc.* **2008**, *130*, 1260.

(10) Jain, V.; Rajbongshi, B. K.; Mallajosyula, A. T.; Bhattacharjya, G.; Iyer, S. K.; Ramanathan, G. *Sol. Energy Mater. Sol. Cells* **2008**, *92*, 1043.

(11) You, Y. J.; He, Y. K.; Borrows, P. E.; Forrest, S. R.; Petasis, N. A.; Thompson, M. E. *Adv. Mater.* **2000**, *12*, 1678.

(12) Polyakov, I.; Epifanovsky, E.; Grigorenko, B. L.; Krylov, A. I.; Nemukhin, A. V. *J. Chem. Theory Comput.* 2009; DOI, 10.1021/ct9001448.

(13) Heim, R.; Prasher, D. C.; Tsien, R. Y. *Proc. Nat. Acad. Sci. U.S.A.* **1994**, *91*, 12501.

(14) Nielsen, S. B.; Lapierre, A.; Andersen, J. U.; Pedersen, U. V.; Tomita, S.; Andersen, L. H. *Phys. Rev. Lett.* **2001**, *87*, 228102.

(15) Andersen, L. H.; Lappierre, A.; Nielsen, S. B.; Nielsen, I. B.; Pedersen, S. U.; Pedersen, U. V.; Tomita, S. *Eur. Phys. J. D* **2002**, *20*, 597.

(16) Ward, W. W.; Cody, C. W.; Hart, R. C.; Cormier, M. J. *Photochem. Photobiol.* **1977**, *31*, 611.

(17) Chattoraj, M.; King, B. A.; Bublitz, G. U.; Boxer, S. G. *Proc. Nat. Acad. Sci. U.S.A.* **1996**, *93*, 8362.

(18) Voityuk, A. A.; Michel-Beyerle, M.-E.; Rösch, N. *Chem. Phys. Lett.* **1997**, *272*, 162.

(19) Weber, W.; Helms, V.; McCammon, J. A.; Langhoff, P. W. *Proc. Nat. Acad. Sci. U.S.A.* **1999**, *96*, 6177.

(20) Helms, V.; Winstead, C.; Langhoff, P. W. *J. Molec. Struct. (Theochem)* **2000**, *506*, 179.

(21) Das, A. K.; Hasegawa, J.-Y.; Miyahara, T.; Ehara, M.; Nakatsuji, H. *J. Comput. Chem.* **2003**, *24*, 1421.

(22) Martin, M. E.; Negri, F.; Olivucci, M. *J. Am. Chem. Soc.* **2004**, *126*, 5452.

(23) Nemukhin, A. V.; Topol, I. A.; Burt, S. K. *J. Chem. Theory Comput.* **2006**, *2*, 292.

(24) Bravaya, K. B.; Bochenkova, A. V.; Granovsky, A. A.; Nemukhin, A. V. *Russ. J. Phys. Chem. B* **2008**, *2*, 671.

(25) Zhang, Y.; Yang, W. *J. Chem. Phys.* **1998**, *109*, 2604.

(26) Polo, V.; Kraka, E.; Cremer, D. *Mol. Phys.* **2002**, *100*, 1771.

(27) Lundber, M.; Siegbahn, P. E. M. *J. Chem. Phys.* **2005**, *122*, 224103.

(28) Dreuw, A.; Weisman, J. L.; Head-Gordon, M. *J. Chem. Phys.* **2003**, *119*, 2943.

(29) Lange, A. W.; Rohrdanz, M. A.; Herbert, J. M. *J. Phys. Chem. B* **2008**, *112*, 6304.

(30) Becke, A. D. *Phys. Rev. A: At., Mol., Opt. Phys.* **1988**, *38*, 3098.

(31) Perdew, J. P. *Phys. Rev. B: Condens. Matter Mater. Phys.* **1986**, *33*, 8822.

(32) Becke, A. D. *J. Chem. Phys.* **1993**, *98*, 5648.

(33) Lee, C.; Yang, W.; Parr, R. G. *Phys. Rev. B: Condens. Matter Mater. Phys.* **1988**, *37*, 785.

(34) Andersson, K.; Malmqvist, P.-Å.; Roos, B. O.; Sadlej, A. J.; Wolinski, K. *J. Phys. Chem.* **1990**, *94*, 5483.

(35) Molina, V.; Merchán, M. *Proc. Nat. Acad. Sci. U.S.A.* **2001**, *98*, 4299.

(36) Andruniów, T.; Ferré, N.; Olivucci, M. *Proc. Nat. Acad. Sci. U.S.A.* **2004**, *101*, 17908.

(37) Murakami, A.; Kobayashi, T.; Goldberg, A.; Nakamura, S. *J. Chem. Phys.* **2004**, *120*, 1245.

(38) Cembran, A.; Bernardi, F.; Olivucci, M.; Garavelli, M. *Proc. Nat. Acad. Sci. U.S.A.* **2005**, *102*, 6255.

(39) Coto, P. B.; Strambi, A.; Ferré, N.; Olivucci, M. *Proc. Nat. Acad. Sci. U.S.A.* **2006**, *103*, 17154.

(40) Frutos, L. M.; Andruniów, T.; Santoro, F.; Ferré, N.; Olivucci, M. *Proc. Nat. Acad. Sci. U.S.A.* **2007**, *104*, 7764.

(41) Schreiber, M.; Barbatti, M.; Zilberg, S.; Lischka, H.; González, L. *J. Phys. Chem. A* **2007**, *111*, 238.

(42) Olsen, S.; Smith, S. C. *J. Am. Chem. Soc.* **2008**, *130*, 8677.

(43) Strambi, A.; Coto, P. B.; Frutos, L. M.; Ferré, N.; Olivucci, M. *J. Am. Chem. Soc.* **2008**, *130*, 3382.

(44) Tokmachev, A. M.; Boggio-Pasqua, M.; Bearpark, M. J.; Robb, M. A. *J. Phys. Chem. A* **2008**, *112*, 10881.

(45) Hirao, K. *Chem. Phys. Lett.* **1992**, *190*, 374.

(46) Nakano, H. *J. Chem. Phys.* **1993**, *99*, 7983.

(47) Nemukhin, A. V.; Bochenkova, A. V.; Bravaya, K. B.; Granovsky, A. A. *Proc. SPIE - Int. Soc. Opt. Eng.* **2007**, *6449*, 64490N.

(48) Bravaya, K.; Bochenkova, A.; Granovsky, A.; Nemukhin, A. *J. Am. Chem. Soc.* **2007**, *129*, 13035.

(49) Perdew, J. P.; Burke, K.; Ernzerhof, M. *Phys. Rev. B: Condens. Matter Mater. Phys.* **1996**, *77*, 3865.

(50) Adamo, C.; Barone, V. *J. Chem. Phys.* **1999**, *110*, 6158.

(51) Dunning, T. H. *J. Chem. Phys.* **1989**, *90*, 1007.

(52) Andersen, L. H.; Bluhme, H.; Boyé, S.; Jørgensen, T. J. D.; Krogh, H.; Nielsen, I. B.; Nielsen, S. B.; Svendsen, A. *Phys. Chem. Chem. Phys.* **2004**, *6*, 2617.

(53) Greemers, T. M. H.; Lock, A. J.; Subramaniam, V.; Jovin, T. M.; Völker, S. *Proc. Nat. Acad. Sci. U.S.A.* **2000**, *97*, 2974.

(54) Jung, G.; Bräuchle, C.; Zumbusch, A. *J. Chem. Phys.* **2001**, *114*, 3149.

(55) Rowe, D. J. *Rev. Mod. Phys.* **1968**, *40*, 153.

(56) Emrich, K. *Nucl. Phys. A* **1981**, *351*, 379.

(57) Sinha, D.; Mukhopadhyay, D.; Mukherjee, D. *Chem. Phys. Lett.* **1986**, *129*, 369.

(58) Stanton, J. F.; Bartlett, R. J. *J. Chem. Phys.* **1993**, *98*, 7029.

(59) Simons, J. Equation of motion (EOM) methods for computing electron affinities. In *Encyclopedia of Computational Chemistry*; J. Wiley & Sons: New York, 2004.

(60) Krylov, A. I. *Annu. Rev. Phys. Chem.* **2008**, *59*, 433.

(61) Livshits, E.; Baer, R. *Phys. Chem. Chem. Phys.* **2007**, *9*, 2932.

(62) Chai, J.-D.; Head-Gordon, M. *J. Chem. Phys.* **2008**, *128*, 084106.

(63) Helgaker, T.; Jørgensen, P.; Olsen, J. *Molecular electronic structure theory*, Wiley & Sons: Chichester, England, 2000.

(64) Granovsky, A. *PC GAMESS*. http://classic.chem.msu.su/gran/gamess/index.html (accessed April 27, 2009).

(65) Schmidt, M. W.; Baldridge, K. K.; Boatz, J. A.; Elbert, S. T.; Gordon, M. S.; Jensen, J. H.; Koseki, S.; Mastunaga, N.; Nguyen, K. A.; Su, S.; Windus, T. L.; Dupuis, M.; Montgomery, J. A. *J. Comput. Chem.* **1993**, *14*, 1347.

(66) Shao, Y.; Molnar, L. F.; Jung, Y.; Kussmann, J.; Ochsenfeld, C.; Brown, S.; Gilbert, A. T. B.; Slipchenko, L. V.; Levchenko, S. V.; O'Neil, D. P.; Distasio, R. A., Jr.; Lochan, R. C.; Wang, T.; Beran, G. J. O.; Besley, N. A.; Herbert, J. M.; Lin, C. Y.; Van Voorhis, T.; Chien, S. H.; Sodt, A.; Steele, R. P.; Rassolov, V. A.; Maslen, P.; Korambath, P. P.; Adamson, R. D.; Austin, B.; Baker, J.; Bird, E. F. C.; Daschel, H.; Doerksen, R. J.; Drew, A.; Dunietz, B. D.; Dutoi, A. D.; Furlani, T. R.; Gwaltney, S. R.; Heyden, A.; Hirata, S.; Hsu, C.-P.; Kedziora, G. S.; Khalliulin, R. Z.; Klunziger, P.; Lee, A. M.; Liang, W. Z.; Lotan, I.; Nair, N.; Peters, B.; Proynov, E. I.; Pieniazek, P. A.; Rhee, Y. M.; Ritchie, J.; Rosta, E.; Sherrill, C. D.; Simmonett, A. C.; Subotnik, J. E.; Woodcock III, H. L.; Zhang, W.; Bell, A. T.; Chakraborty, A. K.; Chipman, D. M.; Keil, F. J.; Warshel, A.; Herhe, W. J.; Schaefer III, H. F.; Kong, J.; Krylov, A. I.; Gill, P. M. W.; Head-Gordon, M. *Phys. Chem. Chem. Phys.* **2006**, *8*, 3172.

(67) Schreiber, M.; Silva-Junior, M. R.; Sauer, S. P. A.; Thiel, W. *J. Chem. Phys.* **2008**, *128*, 134110.

(68) Ghigo, G.; Roos, B. O.; Malmqvist, P.-Å. *Chem. Phys. Lett.* **2004**, *396*, 142.

(69) Christiansen, O.; Koch, H.; Jorgensen, P. *J. Chem. Phys.* **1995**, *103*, 7429.

(70) Koch, H.; Christiansen, O.; Jørgensen, P.; de Meras, A. M. S.; Helgaker, T. *J. Chem. Phys.* **1997**, *106*, 1808.

(71) Grimme, S. *J. Chem. Phys.* **2003**, *118*, 9095.

(72) Jung, Y.; Lochan, R. C.; Dutoi, A. D.; Head-Gordon, M. *J. Chem. Phys.* **2004**, *121*, 9793.

(73) DiStacio, R. A., Jr.; Head-Gordon, M. *Mol. Phys.* **2007**, *105*, 1073.

(74) Rhee, Y. M.; Head-Gordon, M. *J. Phys. Chem. A* **2007**, *111*, 5314.

(75) Iikura, H.; Tsuneda, T.; Yanai, T.; Hirao, K. *J. Chem. Phys.* **2001**, *115*, 3540.

(76) Baer, R.; Neuhauser, D. *Phys. Rev. Lett.* **2005**, *94*, 043002.

(77) Stein, T.; Kronik, L.; Baer, R. *J. Am. Chem. Soc.* **2009**, *131*, 2818–2820.

(78) Pal, S.; Rittby, M.; Bartlett, R. J.; Sinha, D.; Mukherjee, D. *J. Chem. Phys.* **1988**, *88*, 4357.

(79) Stanton, J. F.; Gauss, J. *J. Chem. Phys.* **1994**, *101*, 8938.

(80) Levchenko, S. V.; Krylov, A. I. *J. Chem. Phys.* **2004**, *120*, 175.

(81) Larsen, H.; Hald, K.; Olsen, J.; Jørgensen, P. *J. Chem. Phys.* **2001**, *115*, 3015.

(82) Epifanovsky, E.; Kowalski, K.; Fan, P.-D.; Valiev, M.; Matsika, S.; Krylov, A. I. *J. Phys. Chem. A* **2008**, *112*, 9983.

(83) Hager, B.; Schwarzinger, B.; Falk, H. *Monatsh. Chem.* **2006**, *137*, 163.

(84) Weinhold, F.; Landis, C. R. *Chem. Edu.: Res. Pract. Eur.* **2001**, *2*, 91.

(85) Glendening, E. D.; Badenhoop, J. K.; Reed, A. E.; Carpenter, J. E.; Bohmann, J. A.; Morales, C. M.; Weinhold, F. *NBO 5.0*; Theoretical Chemistry Institute, University of Wisconsin: Madison, WI, 2001.

(86) Slipchenko, L. V.; Krylov, A. I. *J. Chem. Phys.* **2003**, *118*, 6874.

(87) Krylov, A. I.; Sherrill, C. D. *J. Chem. Phys.* **2002**, *116*, 3194.

(88) Simons, J. *J. Phys. Chem. A* **2008**, *112*, 6401.

(89) Simons, J. *Acc. Chem. Res.* **2006**, *39*, 772.

(90) Sobczyk, M. Simons, J. *J. Phys. Chem. B* **2006**, *110*, 7519.

(91) Solntsev, K. M.; Poizat, O.; Dong, J.; Rehault, J.; Lou, Y.; Burda, C.; Tolbert, L. M. *J. Phys. Chem. B* **2008**, *112*, 2700.

(92) Baer, R.; Krylov, A. I. in preparation.

(93) Oana, M.; Krylov, A. I. *J. Chem. Phys.* **2007**, *127*, 234106.

(94) Olsen, S. Ph. D. Thesis, The University of Illinois at Urbana-Champaign, Urbana, IL, 2004.

(95) Stanton, J. F.; Gauss, J. *J. Chem. Phys.* **1999**, *111*, 8785.

(96) Pieniazek, P. A.; Arnstein, S. A.; Bradforth, S. E.; Krylov, A. I.; Sherrill, C. D. *J. Chem. Phys.* **2007**, *127*, 164110.

(97) Hazi, A. U.; Taylor, H. S. *Phys. Rev. A: At., Mol., Opt. Phys.* **1970**, *1*, 1109.

(98) Dong, J.; Abulwerdi, F.; Baldridge, A.; Kowalik, J.; Solntsev, K. M.; Tolbert, L. M. *J. Am. Chem. Soc.* **2008**, *130*, 14096.

CT900143J